EJNMMI Research
a SpringerOpen Journal

ORIGINAL RESEARCH Open Access

Dual time point based quantification of metabolic uptake rates in ^{18}F-FDG PET

Jörg van den Hoff[1,2*], Frank Hofheinz[1], Liane Oehme[2], Georg Schramm[1], Jens Langner[1], Bettina Beuthien-Baumann[2,1], Jörg Steinbach[1] and Jörg Kotzerke[2,1]

Abstract

Background: Assessment of dual time point (DTP) positron emission tomography was carried out with the aim of a quantitative determination of K_m, the metabolic uptake rate of [^{18}F]fluorodeoxyglucose as a measure of glucose consumption.

Methods: Starting from the Patlak equation, it is shown that $K_m \approx m_t/c_a^0 + \bar{V}_r/\tau_a$, where m_t is the secant slope of the tissue response function between the dual time point measurements centered at $t = t_0$. $c_a^0 = c_a(t_0)$ denotes arterial tracer concentration, $\bar{V}_r$ is an estimate of the Patlak intercept, and τ_a is the time constant of the $c_a(t)$ decrease. We compared the theoretical predictions with the observed relation between $K_s = m_t/c_a^0$ and K_m in a group of nine patients with liver metastases of colorectal cancer for which dynamic scans were available, and K_m was derived from conventional Patlak analysis. Twenty-two lesion regions of interest (ROIs) were evaluated. $c_a(t)$ was determined from a three-dimensional ROI in the aorta. Furthermore, the correlation between K_m and late standard uptake value (SUV) as well as retention index was investigated. Additionally, feasibility of the approach was demonstrated in a whole-body investigation.

Results: Patlak analysis yielded a mean V_r of $\bar{V}_r = 0.53 \pm 0.08$ ml/ml. The patient averaged τ_a was 99 ± 23 min. Linear regression between Patlak-derived K_m and DTP-derived K_s according to $K_s = b \cdot K_m + a$ yielded $b = 0.98 \pm 0.05$ and $a = -0.0054 \pm 0.0013$ ml/min/ml ($r = 0.98$) in full accordance with the theoretical predictions $b = 1$ and $a \approx -\bar{V}_r/\tau_a$. K_s exhibits better correlation with K_m than late SUV and retention index, respectively. $K_s^{(c)} = K_s + \bar{V}_r/\tau_a$ is proposed as a quantitative estimator of K_m which is independent of patient weight, scan time, and scanner calibration.

Conclusion: Quantification of K_m from dual time point measurements compatible with clinical routine is feasible. The proposed approach eliminates the issues of static SUV and conventional DTP imaging regarding influence of chosen scanning times and inter-study variability of the input function. K_s and $K_s^{(c)}$ exhibit improved stability and better correlation with the true K_m. These properties might prove especially relevant in the context of radiation treatment planning and therapy response control.

Keywords: Whole-body PET, Dual time point, Metabolic rate of FDG, PET quantification, Tracer kinetic modeling

*Correspondence: j.van_den_hoff@hzdr.de
[1]PET Center, Institute of Radiopharmaceutical Cancer Research, Helmholtz-Zentrum Dresden-Rossendorf, Dresden, 01328, Germany
[2]Department of Nuclear Medicine, University Hospital Carl Gustav Carus, Technische Universität Dresden, Dresden, 01307, Germany

Background

For many years, quantification of the metabolic rate of glucose consumption with dynamic [^{18}F]fluorodeoxyglucose (FDG) positron emission tomography (PET) using the so-called Patlak plot, a procedure most clearly described by Patlak in his seminal papers [1,2], has proven valuable in PET research and clinical routine.

However, in the clinical oncological setting, quantification is mostly restricted to the ubiquitously used standard uptake value (SUV). The reason is twofold: (1) no need (or even inability) to determine the arterial input function (AIF) and (2) inability to perform dynamic whole-body investigations.

Without question, the SUV (defined as the tracer uptake at a certain time point normalized to injected dose per unit body weight) has proven a valuable means of achieving a certain level of quantitative description, thus allowing, e.g., definition of standardized evaluation schemes (see [3] for an overview).

The approach, however, has known shortcomings [4-6]. SUVs do not directly provide information about the tracer kinetics but, by their very nature, only a static snapshot somewhere on the tissue response function (TRF). Naturally, SUVs are varying along the given TRF and are thus prone to variability when not determined at a strictly standardized time. Since SUVs do not contain any information of the actual rate of tracer accumulation (related to the slope of the tissue response function), TRFs from different tissues might in extreme cases even intersect at a certain time (thus exhibiting identical SUVs and zero image contrast at this moment) while having completely different kinetic properties. Tissue SUV stability is further compromised by not accounting for the sizable inter-study variability of arterial blood SUV which directly influences the actually obtained tissue uptake.

One quite extensively investigated way around the 'snapshot problem' is dual time point (DTP) investigations [7,8] in which two successive whole-body scans are performed to obtain information regarding the rate of tracer accumulation. While being undoubtly valuable in discriminating between tumor and inflammation, quantitative evaluation of DTP measurements is usually restricted to computation of a so-called retention index, RI, representing the percentage change of SUV_{max} or SUV_{mean} between early and late images (see, e.g., [9,10]). However, the retention index, too, depends on the acquisition time of (and time difference between) early and late PET scan and, therefore, requires the same strict standardization as the SUV approach to provide useful quantitative measures. The retention index, too, is affected by the mentioned AIF variability at late times due to the evoked changes of the TRF slope.

There also have been attempts to directly use the TRF slope obtained in dynamic scans as a substitute for actual kinetic modeling [11,12] while avoiding measurements of tracer concentration in blood. However, a convincing physiological interpretation of the slope parameter is missing. Furthermore, the approach suffers from the same problems as SUVs and retention index regarding the uncontrolled influence of the inter- and intra-subject variability of the AIF.

In this study, we propose a new assessment of DTP (and, more generally, TRF slope)-based methods with the aim of a quantitative determination of K_m, the metabolic uptake rate of FDG. We demonstrate that starting from the Patlak model, one can derive an analytical relation between K_m and the TRF slope m_t, which only requires the image-based determination of the AIF during the respective late PET scans. The derived relation is especially compatible with dual time point whole-body investigations.

In this retrospective investigation, we evaluate the new approach in a group of patients with liver metastases of colorectal cancer for which K_m was determined, both, by conventional Patlak analysis of the fully dynamic PET scans as well as by the newly developed approach.

Methods

Theory

It is well known that the TRF after a bolus injection of FDG appears to be approximately linear at later times. Closer inspection, however, reveals, that the curve exhibits a finite curvature: the slope decreases with time due to the continuously decreasing AIF (see Figure 1). In the Appendix, we demonstrate that for times t when the Patlak equation is valid (usually for $t > 20 - 30$ min), the ratio between the instantaneous values of TRF slope and AIF level can be expressed in terms of the parameters K_m and V_r of the Patlak model and the time constant τ_a describing the essentially mono-exponential decrease of the AIF in the considered time window. It is shown in the Appendix that the TRF slope at $t = t_0$ is very nearly identical to the slope of the secant connecting the boundary points of a finite symmetric time interval around t_0 (and also to the average slope in this interval).

One finally arrives at the relation

$$K_m = K_s + \frac{V_r}{\tau_a} = \frac{m_t}{c_a^0} + \frac{V_r}{\tau_a} \tag{1}$$

with

$$K_s = \frac{m_t}{c_a^0}, \tag{2}$$

where m_t is the secant (or average) TRF slope in the chosen time interval centered at t_0 and $c_a^0 = c_a(t_0)$ (see Figure 1).

The rate K_s defined by Equation 2 (i.e., the ratio between the TRF slope and AIF level at time t_0) can be determined from measurements during the late phase alone.

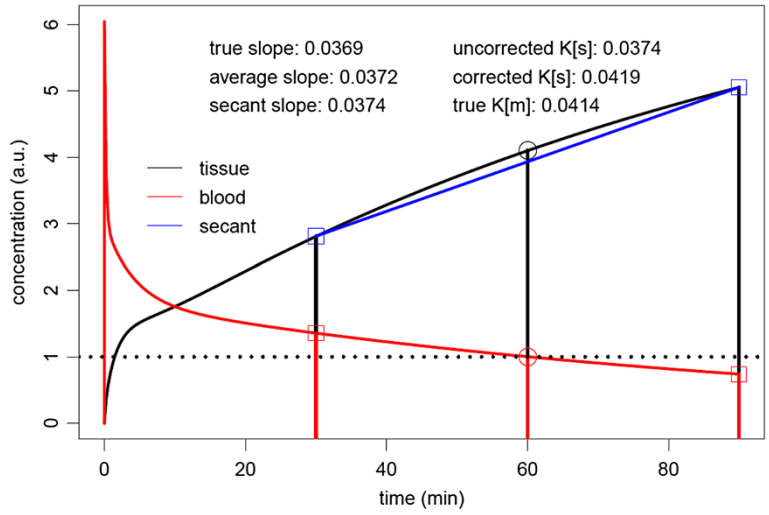

Figure 1 AIF plus TRF calculated for $K_1 = 0.3$ ml/min/ml, $k_2 = 0.5$ /min, $k_3 = 0.08$ /min. The TRF does not become linear at later times but exhibits a visible curvature. However, the slope at some time point t_0 ($t_0 = 60$ min in this example) is nearly identical to the slope of the secant connecting the boundary points of a finite time interval centered at t_0. The AIF is scaled such that $c_a(t_0) = 1$. The data accessible in a DTP measurement are indicated by the square plotting symbols. For further details, see the main text.

Contrary to the Patlak method, knowledge of the full AIF is not required. To the extent that $K_s \gg V_r/\tau_a$, K_s might directly serve as an (negatively biased) approximation of K_m. Moreover, to the extent that V_r can be replaced by a suitable constant value $\bar{V}_r$, K_s differs from K_m only by a τ_a- dependent offset that can be added to K_s to obtain a corrected value

$$K_s^{(c)} = K_s + K_0 = K_s + \frac{\bar{V}_r}{\tau_a} \tag{3}$$

that approximates K_m quite accurately (see Appendix and Figure 1).

We have compared these theoretical predictions with the actually observed relation between K_s and K_m in a group of patients with liver metastases for which fully dynamic scans were performed.

Study sample

The investigated patient group included nine male subjects with liver metastases of colorectal cancer (mean age 62.8 years, range 48 to 76). For each patient, one to three dynamic PET scans of 60 min duration were performed (altogether 15 scans). Scans started immediately after injection of 346 to 430 MBq FDG. The scans were performed with an ECAT EXACT HR$^+$ (Siemens/CTI, Knoxville, TN, USA). The acquired data were sorted into 23 to 31 frames with 10 to 20 s duration during bolus passage, 30 to 150 s duration until 10 min post-injection (p.i.), and 300 s duration afterwards. Tomographic images were reconstructed using attenuation-weighted OSEM reconstruction (6 iterations, 16 subsets, 6 mm FWHM Gaussian filter).

Additionally, feasibility of the generation of parametric $K_s^{(c)}$ maps was demonstrated in a whole-body FDG investigation of a 63-year-old woman with bronchial carcinoma of the right lung and lymph node metastases of the right hilar region and the mediastinum (Philips Ingenuity TF PET/MR (Philips, Cleveland, OH, USA), injected dose 273 MBq, first scan 67 min p.i. (2 min per bed position), second scan 117 min p.i. (1.5 min per bed position)).

Data evaluation

Region of interest (ROI) definition was performed using ROVER (ABX, Radeberg, Germany) [13,14]. The AIF was determined from a roughly cylindrical three-dimensional (3D) ROI centered in the aorta using a concentric safety margin of at least 1 cm to exclude partial volume effects. 3D lesion ROIs were defined in 22 lesions, and the respective TRFs were computed. Further data analysis was performed using the R software for statistical computation [15].

For all 22 lesions, K_m and V_r were derived from the conventional Patlak analysis of the full dynamic data later than 20 min p.i. (at which time all Patlak plots already were linear). For comparison with the corresponding result of the subsequent DTP evaluation, τ_a was determined from a mono-exponential fit to the complete AIF data in the time window used for the Patlak analysis. Variability of τ_a and V_r was expressed as mean $\pm$ standard deviation (SD).

Dual time point data were generated from the data 20 to 30 min and 50 to 60 min p.i., yielding two pairs of c_a and c_t values which were assigned to the respective frame centers $t^{-/+} = 25/55$ min (which corresponds to $t_0 = 0.5 \cdot (t^- + t^+) = 40$ min and $\Delta t = t^+ - t^- = 30$ min).

Using the abbreviations $c_{t/a}^{\pm} = c_{t/a}(t^{\pm})$ and Equation 2, K_s is given by

$$K_s = \frac{m_t}{c_a^0} = \frac{1}{c_a^0} \cdot \frac{\Delta c_t}{\Delta t} = \frac{1}{\sqrt{c_a^- \cdot c_a^+}} \cdot \frac{c_t^+ - c_t^-}{t^+ - t^-}, \qquad (4)$$

where c_a^0 was calculated from the exponential connecting the two points (t^-, c_a^-) and (t^+, c_a^+) which yields $c_a^0 = \sqrt{c_a^- \cdot c_a^+}$.

For $K_s^{(c)}$ computation according to Equation 3, we fixed V_r to the mean of the Patlak evaluation for all lesions ($\bar{V}_r = 0.53$ ml/ml), while τ_a was estimated individually for each study from the exponential connecting (t^-, c_a^-) and (t^+, c_a^+) as

$$\tau_a = \frac{\Delta t}{\ln(c_a^-/c_a^+)}.$$

Additionally, the retention index was computed as $\mathrm{RI} = \Delta c_t / c_t^-$. Linear regression analysis was performed between K_m and K_s, $K_s^{(c)}$, RI, and c_t^+ (the SUV of the lesions in the late image), respectively. Parametric images of K_s, $K_s^{(c)}$, and K_m were generated for visual comparison after filtering of the DTP image data with a bilateral filter [16] (spatial filter width 9 mm, intensity filter width 2.5 SUV).

Influence of image noise

Considering a single voxel and neglecting the (much smaller) statistical error of the ROI-based c_a^0 value, it follows from Equation 4 that the relative statistical error of K_s is equal to that of Δc_t and thus, by Gaussian error propagation,

$$\frac{\sigma_{K_s}}{K_s} = \frac{\sqrt{\left[\sigma_{c_t^+}\right]^2 + \left[\sigma_{c_t^-}\right]^2}}{c_t^+ - c_t^-}$$

which decreases with increasing concentration difference Δc_t. Taking into account that measurement times of both dual time point measurements might be adjusted in such a way that $\sigma_{c_t^-} \approx \sigma_{c_t^+}$, one can get a rough estimate of the error according to

$$\frac{\sigma_{K_s}}{K_s} \approx \sqrt{2} \cdot \frac{\sigma_{c_t^+}}{c_t^+ - c_t^-} = \sqrt{2} \cdot \frac{1}{1 - \frac{c_t^-}{c_t^+}} \cdot \frac{\sigma_{c_t^+}}{c_t^+},$$

where the final ratio represents the relative SUV error of the second dual time point measurement. For $\Delta t \approx 30$ min and typical tumor accumulation rates of $\approx 2\%$ to 4% per minute, one can thus estimate that the relative errors of K_s are about 2.5 to 4 times higher than the corresponding SUV errors (the statistical error of $K_s^{(c)}$ is quite similar since the small correction term $\bar{V}_r/\tau_a$ cannot contribute much to the total statistical uncertainty of $K_s^{(c)}$). Although the noise in the parametric maps can thus be expected to be distinctly higher than that in the uptake images, the resulting visual quality is still quite satisfactory for reasonable choices of Δt ($\gtrsim 30$ min) as will be demonstrated in the following.

Results

The obtained results are summarized in Tables 1 and 2. Figure 2A shows the correlation between Patlak-derived K_m and K_s. The solid line is the line of identity, and the dashed line is the linear regression result. The linear correlation is very good, and the fitted slope is identical to one within the given error limits of about 5% (Table 2). The fitted intercept of −0.54 ml/min/100 ml thus represents the experimentally observed average underestimate of the true K_m by K_s.

Figure 2B presents the correlation between K_m and $K_s^{(c)} = K_s + K_0$ according to Equation 3. The correction term $K_0 = \bar{V}_r/\tau_a$ was computed using the average V_r derived from the Patlak analysis of all 22 lesions, $\bar{V}_r = 0.53$ ml/ml, and individual (investigation-specific) time constants τ_a derived from the DTP data (the independent determination of τ_a from the full dynamic data in the Patlak time window - performed as a consistency check - yielded essentially the same result (104±20 min (dynamic) vs. 99 ± 23 min (DTP)) but was not used further). As can be seen, the degree of linear correlation is distinctly improved in comparison to Figure 2A. Furthermore, the fitted straight line now essentially coincides with the line of identity. Consequently, the average difference between K_m and $K_s^{(c)}$ amounts to only 1.4 ± 4.1% and exceeds 10% only in a single lesion.

For comparison, Figure 3A,B presents the correlations between K_m and the late SUV uptake c_t^+, and K_m and the retention index RI, respectively. Obviously, the correlation between K_m and c_t^+ is rather poor. The correlation between K_m and the RI is substantially higher but still clearly below the degree of correlation between K_m and K_s or $K_s^{(c)}$. The correlation in Figure 3A is clearly distorted by the group of the six highest observed SUV values which correspond to only moderately high K_m values. This phenomenon might be explained by the exceptionally high c_a^0 values observed in the respective patients (see inset graphic in Figure 3A).

Table 1 Summary of parameters entering the K_s and $K_s^{(c)}$ determination

	Mean ± SD	Range
V_r (ml/ml)	0.53 ± 0.08	0.39 − 0.68
Dynamic τ_a (min)	104 ± 20	79 − 156
DTP τ_a (min)	99 ± 23	81 − 172
c_a^0 (SUV)	3.1 ± 0.7	2.4 − 4.5

'Dynamic τ_a' denotes the result derived from the full dynamic AIF data with $t > 20$ min. 'DTP τ_a' was computed solely from the used DTP data. Only the latter was used in further computations.

Table 2 Linear regression results: Pearson correlation coefficient *r* and the obtained regression parameters are shown

	r	Slope (mean ± SD)	Intercept (mean ± SD)
K_m vs. K_s	0.98	0.98 ± 0.05	−0.54 ± 0.13
K_m vs. $K_s^{(c)}$	0.99	0.98 ± 0.04	0.04 ± 0.10
K_m vs. c_t^+	0.60	1.62 ± 0.48	2.81 ± 1.33
K_m vs. RI	0.88	11.38 ± 1.34	5.44 ± 3.79

All correlations were found to be statistically significant with $p < 0.005$. Chosen units are in milliliters per minute per 100 ml for K_m, K_s, and $K_s^{(c)}$; SUV for c_t^+; and percentage for RI (from which the respective slope and intercept units follow).

Figure 4A provides one example of a lesion uptake image, and the corresponding parametric images of K_s, $K_s^{(c)}$, and K_m are shown in Figure 4B,C,D, respectively, all of which are displayed in a common scale. The comparable, enhanced target-to-background contrast of the three parametric images relative to the uptake image is obvious. In agreement with the theoretical expectation and the ROI data in Figure 2, there is good quantitative concordance between K_m and $K_s^{(c)}$, while K_s exhibits a constant negative bias of about $K_0 \approx -0.5$ ml/min/100 ml in comparison to K_m.

Finally, Figure 5 demonstrates the feasibility of generating parametric $K_s^{(c)}$ maps of reasonable statistical quality for a typical DTP whole-body FDG study.

Discussion

Our main result is that in the investigated patient group, there is a very pronounced linear correlation $K_s = a + b \cdot K_m$, where b is very nearly equal to one (see Figure 2A). This behavior is in complete agreement with the formalism presented in the Appendix, notably Equation 13: the variations of the (small) term V_r/τ_a should be essentially uncorrelated to K_m so that a high (but slightly "noisy") linear correlation between K_m and K_s with a slope near one is predicted. Furthermore, according to Equation 13, the modulus of the intercept, $a = -0.0054$ ml/min/ml, should be approximately equal to the average of V_r/τ_a in the investigated patient group. This prediction, too, is in complete agreement with the actual values of V_r (determined from Patlak analysis) and τ_a, namely $\bar{V}_r = (0.53 \pm 0.08)$ ml/ml and $\bar{\tau}_a = (99 \pm 23)$ min.

The second important finding is the fact that the degree of correlation as well as quantitative agreement between K_m and K_s can be further improved by assuming a reasonable constant value for $\bar{V}_r$ (since V_r is inaccessible in DTP measurements) and determining individually the rate of decrease, τ_a, of the AIF (which can be estimated from the DTP measurement). The corrected K_s, $K_s^{(c)} = K_s + \bar{V}_r/\tau_a$, exhibits an improved correlation to K_m (due to compensation of the τ_a variability) and also improved quantitative concordance as long as $\bar{V}_r$ is roughly in accord with the individual true V_r. Both phenomena are illustrated clearly in Figure 2B. The distinctly improved correlation (compared to Figure 2A) is achieved by the individual correction of the τ_a influence. The residual deviations from the perfect correlation in Figure 2B are mainly due to the variability of V_r. A nearly perfect quantitative agreement with K_m is observed since $\bar{V}_r$ was set to the mean of the actual V_r values derived from the Patlak analysis. This obviously would not be possible when considering realistic DTP measurements (without a preceding complete dynamic study), and a less-than-perfect quantitative agreement should be expected in this case. Nevertheless, as the comparison of Figure 2A,B suggests, performing the correction with some roughly correct value for $\bar{V}_r$ will always decrease the bias between K_s and K_m.

The rather small variability of tumor V_r observed in the present investigation might seem surprising. However, the square of $k_2/(k_2 + k_3)$ appearing in Equation 6 will never deviate very much from unity since for FDG, k_2 quite

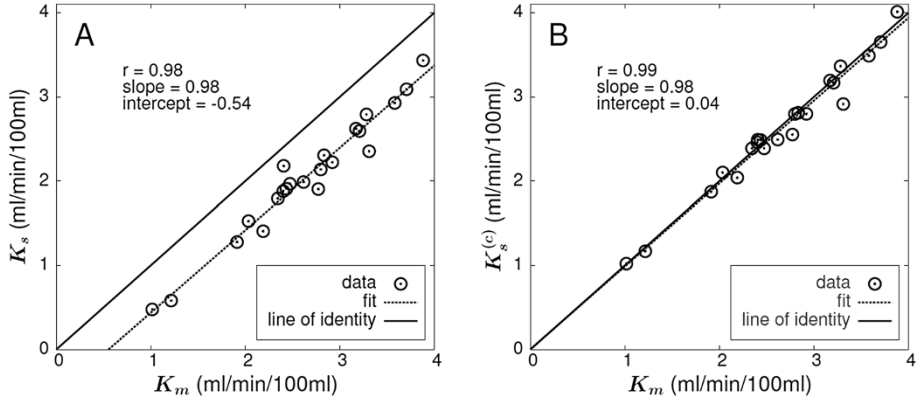

Figure 2 Correlation between the metabolic rate K_m and the DTP-derived rate constants. (A) K_m and K_s and **(B)** K_m and $K_s^{(c)}$. Solid black lines represent the line of identity; dashed lines represent the least squares straight line fits to the data.

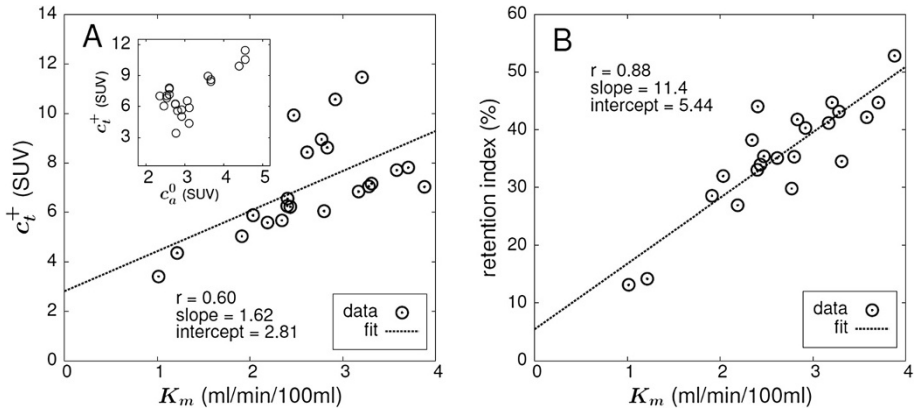

Figure 3 Correlation between the metabolic rate K_m and Standard Uptake Value and retention index, respectively. (A) K_m and c_t^+ (in SUV units) and (B) K_m and retention index (in percent). c_t^+ is the tissue uptake at $t = 55$ min. Dashed lines represent the least squares straight line fits to the data. The inset graph in (A) additionally provides the correlation between c_a^0 and c_t^+, which helps to explain the group of data points above the regression line with SUV>8 (see the 'Discussion' section).

generally is distinctly larger than k_3. The variability of V_r is thus mostly controlled by the first term, K_1/k_2. Since both K_1 and k_2 are usually identified as being associated with the facilitated diffusion across the cell membrane, it might very well be expected that the ratio K_1/k_2 is essentially constant, independent of the actual K_1. This might be the underlying reason for the low variability of V_r observed in this study. Whether V_r variability is higher in other tumors remains to be investigated, but we believe this to be unlikely. V_r should never be much larger than about 0.6 to 0.7 ml/ml which appears to be a rough upper bound for the K_1/k_2 ratio. According to our own data, this is true, e.g., in the human brain ($K_1/k_2 \approx 0.1/0.15 = 0.67$ ml/ml) as well as the myocardium ($K_1/k_2 \approx 0.6/1.4 = 0.43$ ml/ml). V_r in these organs is rather low (≈ 0.3 ml/ml) due to the large k_3 in both tissues.

We surmise, therefore, that V_r in tumors (and healthy tissue) will never deviate too much from the value of 0.53, ml/ml used for K_s correction in this study. The corrected rate, $K_s^{(c)}$, can then be expected to be a less biased estimate of K_m than K_s over a substantial range of actually realized V_r values between about 0.2 and 0.7 ml/ml (see Figures 6 and 7). Whether $K_s^{(c)}$ does offer any advantages over K_s in terms of clinical relevance remains to be seen, but the improved correlation with K_m seems justification enough to perform the correction.

The very high correlation between $K_s^{(c)}$ (or K_s) and K_m is to be compared with the markedly inferior correlation between K_m and late SUV (c_t^+) and retention index RI, respectively (Figure 3). Since all these parameters are ultimately intended as surrogate parameters of K_m, the superiority of K_s seems obvious. Since in the present study the retention index is computed from exactly the same DTP tissue data as K_s, it is worth to point out that the sole factor responsible for the much better $K_s(K_m)$ correlation is adequate consideration of the substantial inter-subject c_a^0 variability (see Table 1). Indeed, one could write $K_s = \Delta c_t/\Delta t/c_a^0 = \Delta c_t/c_t^-/\Delta t \cdot c_t^-/c_a^0 = RI/\Delta t \cdot c_t^-/c_a^0$, where Δt is just a constant in the present context. To some extent, K_s might thus be considered just a more sensible definition of a retention index where the uptake difference Δc_t is normalized to c_a^0 (as well as Δt) instead of c_t^-.

The observed very low correlation between late SUV and K_m is caused by the six data points with SUV>8 in Figure 3A. Leaving these six points out increases

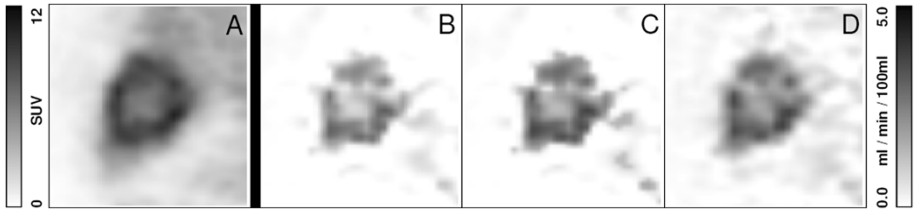

Figure 4 Liver metastasis of a colorectal carcinoma exhibiting a central necrosis. (**A**) A representative sagittal slice of uptake and the corresponding parametric images of (**B**) K_s, (**C**) $K_s^{(c)}$, and (**D**) K_m, respectively, are shown. The means of the rate constants over the lesion are as follows: $K_s = 2.23$ ml/min/100 ml, $K_s^{(c)} = 2.80$ ml/min/100 ml, and $K_m = 2.90$ ml/min/100 ml, demonstrating a quite satisfactory quantitative agreement between $K_s^{(c)}$ and K_m.

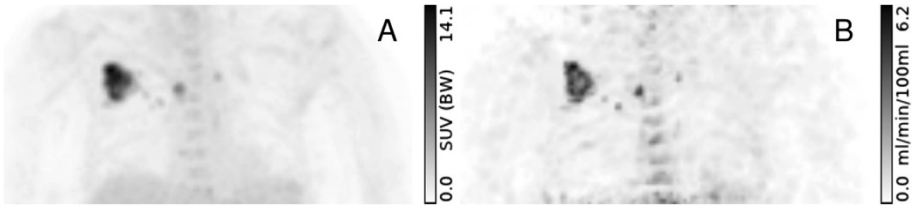

Figure 5 Comparison of parametric images of SUV and $K_s^{(c)}$. (A) FDG SUV 67 min. p.i. and **(B)** parametric $K_s^{(c)}$ map in a 63-year-old woman. The patient has a bronchial carcinoma of the right lung and lymph node metastases of the right hilar region and the mediastinum (coronal maximum projection). Note the different regional contrast and the used units in both images.

the correlation coefficient to 0.94 which is in good agreement with published data [17]. Closer inspection revealed exceptionally high c_a^0 values (see inset graphic in Figure 3A) for the affected data points which might have physiological reasons but could also hint at erroneous SUV calibration (for which, however, a retrospective inspection did not find any evidence). In any case, the data demonstrate the high sensitivity of SUV evaluations to variations of the AIF level and incorrect SUV calibration.

The comparison of uptake and parametric images in Figure 4 demonstrates that K_s as well as $K_s^{(c)}$ reproduces the essential features of the Patlak K_m image, notably the increased contrast between metastasis and liver background. Regarding the targeted lesions, the $K_s^{(c)}$ image is, moreover, in good quantitative agreement with the K_m image and could thus serve as a basis for regional quantitative evaluation. We, therefore, believe it is worthwhile to investigate the potential suitability of $K_s^{(c)}$ as a quantitative estimator (and not just a surrogate) of K_m more thoroughly in future studies. Figure 5 demonstrates that reasonable statistical quality of the $K_s^{(c)}$ map can in fact be achieved in whole-body DTP investigations as well.

Compared to more conventional approaches, our approach has several relevant benefits. The most important one in our view is the potential to perform fully

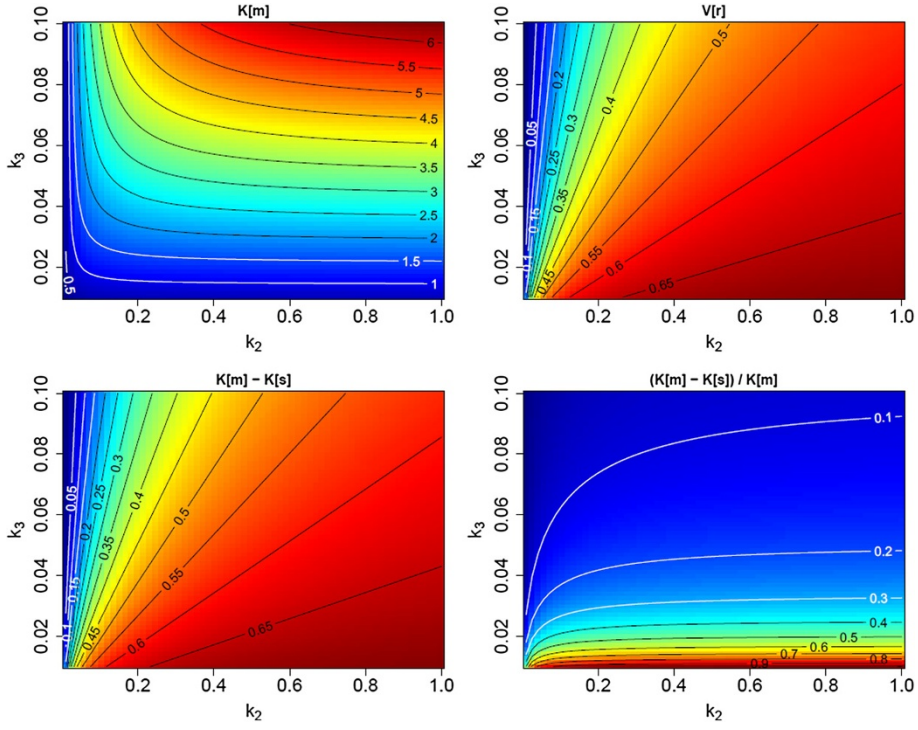

Figure 6 Visualization of the difference between K_m and K_s. The plots cover a substantial range of the parameters k_2 and k_3, assuming a fixed ratio $K_1/k_2 = 0.7$ ml/ml (a rationale for fixing this ratio is given in the discussion above). Top left, K_m; top right, V_r; bottom left, absolute difference $(K_m - K_s)$; and bottom right, fractional difference $((K_m - K_s)/K_m)$. Parameters and their respective units: k_2, k_3 (1/min); V_r (ml/ml); and K_m, K_s (ml/min/100 ml). Moving along the line, $V_r \approx 0.55$ ml/ml between $K_m = 1$ and 4 ml/min/100 ml corresponds approximately to the experimental data of Figure 2A.

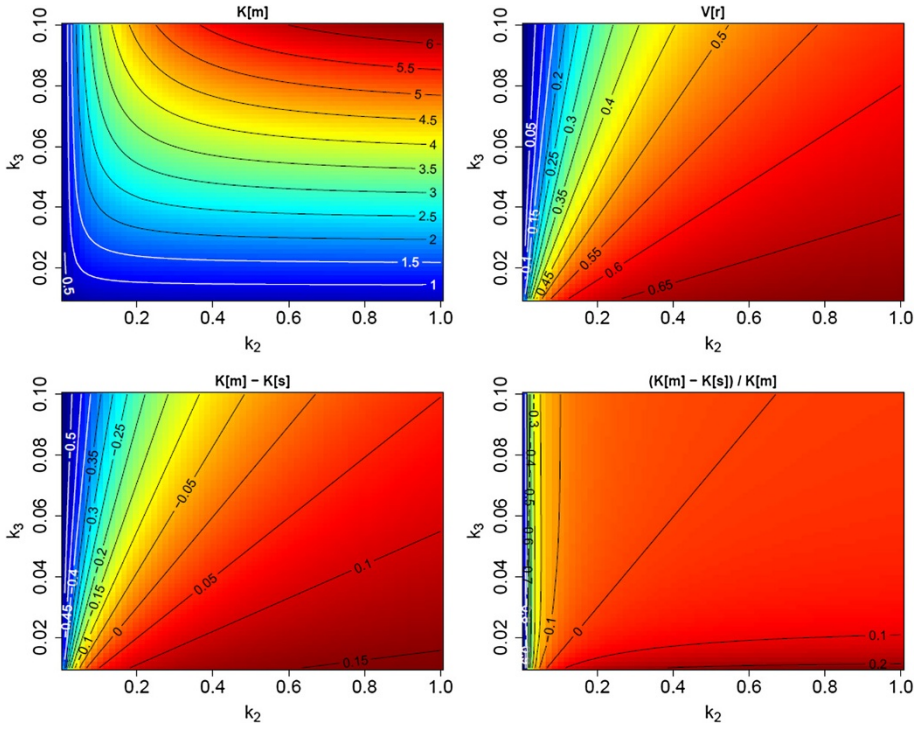

Figure 7 Visualization of the difference between K_m and $K_s^{(c)}$ for $\tau_a = 99$ min and an assumed distribution volume $\bar{V}_r = 0.53$ ml/ml. In comparison with Figure 6, the systematic difference relative to the true K_m is mostly removed even when V_r deviates distinctly from the assumed value. Moving along the line, $V_r \approx 0.55$ ml/ml between $K_m = 1$ and 4 ml/min/100ml corresponds approximately to the experimental data of Figure 2B.

quantitative whole-body investigations based on a DTP acquisition. The only additional prerequisite is identification of the aorta or left ventricle in the DTP data. One gains the ability to directly identify regions of elevated irreversible FDG metabolism and to put the established DTP approach on a quantitative basis. A further advantage is the implied correction for the sizable inter-subject variation of the blood tracer concentration (SUV range, $2.4 - 4.5$ in this study). The latter correction alone clearly improves the correlation between the derived parameter (K_s) and the targeted one (K_m). Another important aspect is elimination of the dependence of SUV uptake and retention index on the time of measurement(s). To the extent that the Patlak model can be considered valid (negligible k_4), the proposed procedure yields a time-independent result, namely a direct estimate of the invariant rate K_m which prospectively should allow definition of improved, objective reference values. A further implication is elimination of any intra-scan time dependence in whole-body/multi-bed studies. Last but not least, the issue of ensuring correct SUV calibration is eliminated since all calibration factors cancel out when performing an image-based determination of both TRF slope and c_a^0. This observation seems especially relevant for multi-center studies.

Conclusion

We have demonstrated that it is possible to derive a quantitative estimate of K_m, the metabolic trapping rate of FDG, solely from a dual time point measurement. We believe this approach to be of potential relevance especially in the context of oncological whole-body investigations where the required AIF information is available in the field of view (aorta or left ventricle). In this case, the approach eliminates most if not all issues of static SUV and conventional dual time point imaging regarding the influence of the chosen scan times relative to the time of injection and the substantial influence of inter-study variability of the AIF. Consequently, the derived parameters K_s and $K_s^{(c)}$ exhibit a much improved stability and much better correlation with the true K_m. These properties might prove especially relevant in the context of radiation treatment planning and therapy response control. Whether this is indeed the case has to be investigated in appropriate future studies.

Appendix

We start with the standard Patlak formula but avoid division by $c_a(t)$:[a]

$$c_t(t) = K_m \cdot \int_0^t c_a(s)ds + V_r \cdot c_a(t), \tag{5}$$

where K_m is the metabolic trapping rate, defined by

$$K_m = \frac{K_1 k_3}{k_2 + k_3}$$

and V_r is the apparent volume of distribution defined by

$$V_r = \frac{K_1 k_2}{(k_2 + k_3)^2} = \frac{K_1}{k_2} \cdot \left(\frac{k_2}{k_2 + k_3} \right)^2 . \tag{6}$$

Equation 5 is valid for times $t > T^*$ where $T^* \approx 20$ to 30 min p.i.. Utilization of this equation for K_m determination requires measurements of the TRF only for $t > T^*$ but measurement of the complete AIF starting at time zero. We now want to eliminate the dependency on measurements prior to T^*. By taking the time derivative at some time point $t > T^*$, it follows directly from Equation 5 that

$$\dot{c}_t(t) = K_m \cdot c_a(t) + V_r \cdot \dot{c}_a(t)$$

or after division by $c_a(t)$ (suppressing the t argument)

$$\frac{\dot{c}_t}{c_a} = K_m + V_r \cdot \frac{\dot{c}_a}{c_a}. \tag{7}$$

Focusing on some specific time point $t = t_0$, we use the Taylor expansion of $c_a(t)$ around t_0 ($c_a^{(n)}(t_0)$: nth derivative at $t = t_0$):

$$c_a(t) = \sum_{n=0}^{\infty} \frac{c_a^{(n)}(t_0)}{n!} (t - t_0)^n. \tag{8}$$

Introducing the parameters τ_n defined by $(-\tau_n)^n = c_a^0 / c_a^{(n)}(t_0)$, Equation 8 can be rewritten as

$$\begin{aligned} c_a(t) &= c_a^0 \cdot \sum_{n=0}^{\infty} \frac{(-1)^n}{n!} \left(\frac{t - t_0}{\tau_n} \right)^n \\ &= c_a^0 \cdot \left(1 - \frac{t - t_0}{\tau_1} + \frac{1}{2!} \left(\frac{t - t_0}{\tau_2} \right)^2 - \dots \right), \end{aligned} \tag{9}$$

where τ_0 is always equal to one. The parameters $\tau_{n>0}$ are constructed in such a way that for a mono-exponential decrease of $c_a(t)$ near t_0, we obtain $\tau_{n>0} = \tau_a$, where τ_a is the time constant of the exponential. Actually, it is known that starting rather early after bolus injection ($t > 20$ min), $c_a(t)$ can be reasonably well described by a slow mono-exponential decrease with a time constant $\tau_a \approx 100$ min (in the present study, we found an average value of $\tau_a = 99$ min, while a value of $\tau_a = 80$ min was reported in [18]).

Inserting the Taylor expansion from Equation 9 into Equation 7, we get ($\dot{c}_t^0 = \dot{c}_t(t_0)$)

$$\frac{\dot{c}_t^0}{c_a^0} = K_m - \frac{V_r}{\tau_1}. \tag{10}$$

In order to derive K_m from this equation, we need to reliably estimate $\dot{c}_t^0 / c_a^0$ as well as to have knowledge of $1/\tau_1$ (the fractional rate of decrease of the AIF at $t = t_0$). Obviously, direct determination of the time derivative $\dot{c}_t^0$ at $t = t_0$ is not feasible in real (noisy) data. On the other hand, it is not clear whether the average slope over a necessarily rather large neighborhood (required for reasons of limited time resolution and count rate statistics) is an acceptable approximation of $\dot{c}_t^0$ (since the slope changes over time). For investigation of this question, we compute from Equation 5 the difference $c_t^+ - c_t^- = c_t\left(t_0 + \frac{\Delta t}{2}\right) - c_t\left(t_0 - \frac{\Delta t}{2}\right)$ for two time points lying symmetrically around t_0 at a finite (possibly large) distance Δt

$$\Delta c_t(\Delta t) = c_t^+ - c_t^- = K_m \cdot \int_{t_0 - \frac{\Delta t}{2}}^{t_0 + \frac{\Delta t}{2}} c_a(s) ds + V_r \cdot \left(c_a^+ - c_a^- \right) \tag{11}$$

with $c_a^{\pm} = c_a\left(t_0 \pm \frac{\Delta t}{2}\right)$.

Replacing all occurrences of $c_a(t)$ in Equation 11 by the Taylor series in Equation 9 (neglecting fourth and higher order terms) and executing the integration separately for each term of the series yield after some straightforward but lengthy calculations the following equation:

$$\begin{aligned} \Delta c_t = \Bigg(& K_m \left[1 + \frac{1}{24} \left(\frac{\Delta t}{\tau_2} \right)^2 \right] \\ & - \frac{V_r}{\tau_1} \left[1 + \frac{1}{24} \frac{\tau_1}{\tau_3} \left(\frac{\Delta t}{\tau_3} \right)^2 \right] \Bigg) c_a^0 \cdot \Delta t \end{aligned} \tag{12}$$

The detailed derivation of Equation 12 is presented in an additional file (see Additional file 1). The factors in square brackets deviate only minimally from one up to even quite large values of Δt. For the sake of simplicity, we will demonstrate this only for the well-established approximately mono-exponential behavior of $c_a(t)$ at later times but emphasize that the conclusions remain the same when using other reasonable parametrizations of the observed shape of the AIF at later times (e.g., by an inverse power law).

As already pointed out, for a mono-exponential decrease of $c_a(t)$, all $\tau_{n>0}$ coincide with the time constant τ_a of the exponential. Consider, then, choosing $\Delta t = 60$ min in Equation 12 . Since $\tau_a \approx 100$ min, we have for both square brackets $1 + 1/24 \cdot 0.6^2 = 1.015$. It is, therefore, permissible to replace both square brackets by one. This yields

$$\Delta c_t \approx \left[K_m - \frac{V_r}{\tau_a} \right] c_a^0 \cdot \Delta t.$$

Thus, Δc_t is to a very good approximation proportional to Δt. Δt can become quite large, e.g., $\Delta t = 1$ h, as long as

the lower bound $t_0 - \frac{\Delta t}{2}$ remains larger than T^*. Defining the secant slope m_t between c_t^- and c_t^+

$$m_t = \frac{\Delta c_t}{\Delta t}$$

and introducing the rate constant K_s

$$K_s = \frac{m_t}{c_a^0}$$

for the ratio of the secant slope and the blood concentration at t_0, we get

$$K_s = \frac{m_t}{c_a^0} = K_m - \frac{V_r}{\tau_a} \tag{13}$$

or

$$K_m = K_s + \frac{V_r}{\tau_a}. \tag{14}$$

Comparison of Equation 13 with Equation 10 yields the important result

$$m_t = \dot{c}_t^0.$$

In other words, the secant slope is to a very good approximation equal to the instantaneous slope at t_0 and thus can be used instead. This in turn implies that the average slope of the TRF (derivable, e.g., by a least squares fit of a straight line in the considered time window), too, is very nearly identical to m_t. Note that these conclusions are valid even if $\dot{c}_t(t)$ varies considerably over the considered time interval (see Figure 1). Formally, this result is identical to stating that a second-order Taylor expansion of $c_t(t)$ around t_0 turns out to be sufficiently accurate within $t_0 \pm \Delta t/2$.

The quantitative relation between K_s and K_m is investigated in Figure 6. For this figure, we computed K_m and V_r over a range of sensible choices for the transport constants K_1, k_2, and k_3. The resulting K_m and V_r (top row of Figure 6) are used to compute K_s from Equation 13 for a realistic value of τ_a (we chose $\tau_a = 99$ min). The bottom row in Figure 6 compares the true K_m to K_s.

As can be seen (bottom right), the fractional deviation of K_s from K_m becomes large only when k_3 is very small (i.e., when there is virtually no trapping). Overall K_s is a negatively biased estimator of K_m, but an approximate correction of the bias is possible considering the following.

According to Equation 14, theV_r and $K_m - K_s$ maps in Figure 6 differ only by a constant factor τ_a (and a conversion factor of 100 due to the chosen units of ml/min/100 ml for K_m and K_s). Moreover, V_r does vary only modestly in comparison to the individual rate constants and to K_m (except when k_3 becomes distinctly larger than k_2, but this is not observed in real data). Therefore, $K_m - K_s$ does not vary much across the relevant part of the k_2/k_3 plane. We, therefore, hypothesize that the difference $K_m - K_s$ can be actually treated to be approximately constant. Consequently, we propose to estimate K_m using only late time measurements of $c_a(t)$ and $c_t(t)$ as follows:

1. Determine the secant TRF slope m_t in the time interval $t^{\pm} = t_0 \pm \frac{\Delta t}{2}$ from a dual time point measurement of $c_t(t)$ starting at sufficiently late times after injection, typically $t > (20 - 30)$ min.
2. Estimate $c_a^0 = c_a(t_0)$ and τ_a from the exponential connecting the two time points t^-, t^+.
3. Compute $K_s = m_t/c_a^0$.
4. Compute a correction term $K_0 = \bar{V}_r/\tau_a$ using the individually determined τ_a and a fixed value $\bar{V}_r$ for the distribution volume. In the absence of any specific information regarding V_r in the investigated tumor entity, we propose to use the average V_r determined in this study, i.e., $\bar{V}_r = 0.53$ ml/ml.
5. Finally, compute the corrected K_s, i.e.,

$$K_s^{(c)} = K_s + K_0 = K_s + \bar{V}_r/\tau_a \tag{15}$$

as a quantitative estimate of the true K_m.

According to Equations 14 and 15, $K_s^{(c)}$ is equal to K_m if $V_r = \bar{V}_r$ (irrespective of the values of K_1- k_3 yielding this V_r value). Therefore, $K_s^{(c)}$ remains a very good approximation of K_m as long as V_r does not deviate too much from the assumed value. This behavior is illustrated in Figure 7.

Endnote

[a]For completeness, we mention that in the presence of sizable fractional blood volume (*fbv*), the substitutions $K_m \to K_m^* = (1 - fbv)K_m$ and $V_r \to V_r^* = (1 - fbv)V_r + fbv = V_r + fbv(1 - V_r)$ would have to be performed in Equation 5 where the 'asterisked' quantities would be the experimentally accessible ones.

Additional file

Additional file 1: Derivation of Equation 12. A pdf file showing the complete derivation of Equation 12 using Taylor expansion.

Competing interests
The authors declare that they have no competing interests.

Authors' contributions
JVDH derived the theoretical background, performed part of the data analysis, and is the main author of the manuscript. FH performed part of the data analysis and wrote part of the manuscript. LO and GS contributed to the derivation of the theoretical background. JL and BBB performed the PET measurements. JS and JK provided intellectual input and reviewed the manuscript. All authors read and approved the final manuscript.

Received: 10 January 2013 Accepted: 12 February 2013
Published: 13 March 2013

References

1. Patlak C, Blasberg R, Fenstermacher J: **Graphical evaluation of blood-to-brain transfer constants from multiple-time uptake data.** *J Cereb Blood Flow Metab* 1983, **3:**1–7.

2. Patlak C, Blasberg R: **Graphical evaluation of blood-to-brain transfer constants from multiple-time uptake data. Generalizations.** *J Cereb Blood Flow Metab* 1985, **5**(4):584–590.
3. Wahl R, Jacene H, Kasamon Y, Lodge M: **From RECIST to PERCIST: evolving considerations for PET response criteria in solid tumors.** *J Nucl Med* 2009, **50**(Suppl 1):122S–150S.
4. Hamberg L, Hunter G, Alpert N, Choi N, Babich J, Fischman A: **The dose uptake ratio as an index of glucose metabolism: useful parameter or oversimplification?** *J Nucl Med* 1994, **35**(8):1308.
5. Keyes JJr: **SUV: standard uptake or silly useless value?** *J Nucl Med* 1995, **36**(10):1836–1839.
6. Huang S: **Anatomy of SUV.** *Nucl Med Biol* 2000, **27**(7):643–646.
7. Hustinx R, Smith R, Benard F, Rosenthal D, Machtay M, Farber L, Alavi A: **Dual time point fluorine-18 fluorodeoxyglucose positron emission tomography: a potential method to differentiate malignancy from inflammation and normal tissue in the head and neck.** *Eur J Nucl Med Mol Imaging* 1999, **26**(10):1345–1348.
8. Zhuang H, Pourdehnad M, Lambright E, Yamamoto A, Lanuti M, Li P, Mozley P, Rossman M, Albelda S, Alavi A: **Dual time point 18F-FDG PET imaging for differentiating malignant from inflammatory processes.** *J Nucl Med* 2001, **42**(9):1412–1417.
9. Basu S, Alavi A: **Partial volume correction of standardized uptake values and the dual time point in FDG-PET imaging: should these be routinely employed in assessing patients with cancer?** *Eur J Nucl Med Mol Imaging* 2007, **34**(10):1527–1529.
10. Lin Y, Chen J, Ding H, Liang J, Yeh J, Kao C: **Potential value of dual-time-point 18F-FDG PET compared with initial single-time-point imaging in differentiating malignant from benign pulmonary nodules: a systematic review and meta-analysis.** *Nucl Med Commun* 2012, **33**(10):1011–1018.
11. Strauss L, Klippel S, Pan L, Schönleben K, Haberkorn U, Dimitrakopoulou-Strauss A: **Assessment of quantitative FDG PET data in primary colorectal tumours: which parameters are important with respect to tumour detection?** *Eur J Nucl Med Mol Imaging* 2007, **34**(6):868–877.
12. Herzog H, Meyer P, Stoffels G, Floeth F, Coenen H, Langen K: **Simplified analysis of FET-kinetics in brain tumors by voxel-by-voxel linear regression.** *J Nucl Med* 2008, **49**(Suppl 1):78P.
13. ROVER: **ROVER: ROI visualization, evaluation and image registration.** ABX Radeberg 2008. [http://www.abx.de/rover].
14. Hofheinz F, Pötzsch C, Oehme L, Beuthien-Baumann B, Steinbach J, Kotzerke J, van den Hoff J: **Automatic volume delineation in oncological PET Evaluation of a dedicated software tool and comparison with manual delineation in clinical data sets.** *Nuklearmed* 2012, **51:**9–16.
15. R Development Core Team: *R: A Language and Environment for Statistical Computing*. Vienna: R Foundation for Statistical Computing; 2011. [http://www.R-project.org].
16. Hofheinz F, Langner J, Beuthien-Baumann B, Oehme L, Steinbach J, Kotzerke J, van den Hoff J: **Suitability of bilateral filtering for edge-preserving noise reduction in PET.** *EJNMMI Res* 2011, **1:**1–9.
17. Freedman N, Sundaram S, Kurdziel K, Carrasquillo J, Whatley M, Carson J, Sellers D, Libutti S, Yang J, Bacharach S: **Comparison of SUV and Patlak slope for monitoring of cancer therapy using serial PET scans.** *Eur J Nucl Med Mol Imaging* 2003, **30:**46–53.
18. Buchert R, van den Hoff J, Mester J: **Accurate determination of metabolic rates from dynamic positron emission tomography data with very-low temporal resolution.** *J Comput Assist Tomo* 2003, **27**(4):597–605.

doi:10.1186/2191-219X-3-16
Cite this article as: van den Hoff *et al.*: Dual time point based quantification of metabolic uptake rates in ^{18}F-FDG PET. *EJNMMI Research* 2013 **3**:16.